Materials Science & Engineering A 564 (2013) 324–330

Contents lists available at SciVerse ScienceDirect

Materials Science & Engineering A

journal homepage: www.elsevier.com/locate/msea

Thermal barrier coating toughness: Measurement and identification of a bridging mechanism enabled by segmented microstructure

Erin M. Donohue [a,*], Noah R. Philips [a], Matthew R. Begley [a,b], Carlos G. Levi [a,b]

[a] Materials Department, University of California, Santa Barbara, United States
[b] Mechanical Engineering Department, University of California, Santa Barbara, United States

ARTICLE INFO

Article history:
Received 18 September 2012
Received in revised form
27 November 2012
Accepted 30 November 2012
Available online 8 December 2012

Keywords:
Toughness
Thermal barrier coatings
Yttria-stabilized zirconia
Fracture mechanisms
Crack bridging

ABSTRACT

Failure mechanisms in thermal barrier coatings (TBCs) often involve the propagation of delamination cracks within the top coating. The work presented in this paper makes two principal contributions: first, the development of a straightforward testing geometry and analysis approach enables the accurate determination of the mode I fracture toughness of these coatings and second, the application of the approach to technologically relevant coatings produces new insights into the impact of the dense vertically cracked (DVC) microstructure on the toughness. Mode I toughness of air plasma-sprayed 8 wt% yttria-stabilized zirconia DVC TBCs is measured by sandwiching the freestanding coatings in a modified double cantilever beam configuration. Digital image correlation measurements and finite element analysis provide a pathway to quickly and accurately extract toughness values from displacement data alone. Results show R-curve behavior and unexpectedly high steady-state toughness values of $G_{ss} \approx 300-400\ \mathrm{J/m^2}$. The observation of this elevated toughness can be rationalized by a crack bridging model that is consistent with the TBC's starting microstructure and features of the fracture surfaces.

1. Introduction

Thermal barrier coatings (TBCs) are key components of multi-layered thermal protection systems in gas turbines, which enable greater fuel efficiency by allowing operation at increased temperatures [1,2]. The lifetime of a coating is often strongly dependent on its toughness, a property that determines the extent of various failure mechanisms [2], both intrinsic (e.g. thickening or rumpling of the thermally grown oxide [3–7]) and extrinsic (e.g. impact damage [8–11] and cracking due to molten siliceous deposits [12–15]). Hence, predictions of coating durability and design of future TBCs often rely critically on an accurate assessment and understanding of toughness.

While the importance of measuring TBC toughness is clear [10,14], there are relatively few direct measurements on pertinent microstructures [16–18]. (Indirect assessments on the intrinsic toughness of the appropriate composition, 8 wt% yttria-stabilized zirconia (8YSZ), include [19–21]). Coatings examined in this article are produced by air plasma spray (APS) and contain segmented cracks in the thickness direction to provide greater strain tolerance upon thermal cycling (Fig. 1) [22–25]. While standard APS coatings are highly porous to attain low thermal conductivity, the processing conditions to create the segmented cracks cause the intervening material to have significantly less porosity [26]. Referred to as dense vertically cracked (DVC) microstructures, these coatings can still maintain a sufficiently high thermal gradient in operation [25,26]. In order to probe the behavior of materials used in actual turbines, the difficult task of fabricating suitable fracture specimens from thin, freestanding, ceramic coatings must be overcome.

Here, fracture experiments are conducted using a modified double cantilever beam (DCB) geometry, where the TBC is sandwiched between two steel beams and tested in displacement control via wedge loading (Fig. 2). Quantification of R-curve behavior is possible provided that (i) the crack tip can be correctly determined as a function of the beam deflection and (ii) the energy release rate can be calculated accurately while accounting for complicating factors such as the finite compliance of the ceramic layer and transverse shear effects. These interrelated challenges are addressed by the combination of digital image correlation (DIC) measurements and finite element (FE) analysis.

A key insight in the present approach, which facilitates the extraction of the crack tip location from DIC data, is that the centerline of the beams experiences negative displacements just ahead of the crack tip (Fig. 2). This feature is observed in both the FE results and analytical models of beams on finite-sized elastic foundations (i.e. the length of the TBC in the sandwich). In both analyses, it is revealed that the distance between the onset of the

* Corresponding author. Fax: +1 805 893 8486.
E-mail address: erin_donohue@engineering.ucsb.edu (E.M. Donohue).

0921-5093/$ - see front matter © 2012 Elsevier B.V. All rights reserved.
http://dx.doi.org/10.1016/j.msea.2012.11.126

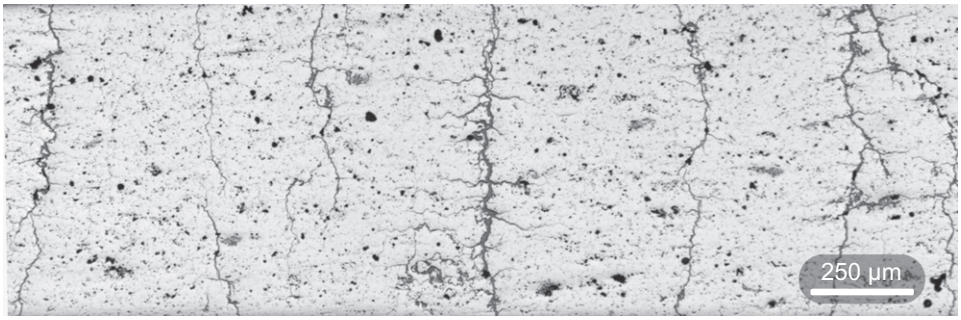

Fig. 1. A cross-sectional view of an 8YSZ APS coating with a segmented microstructure comprising of through-thickness cracks that form an in-plane mud cracking pattern, which define pillar-like features that enable the toughening mechanism discussed herein.

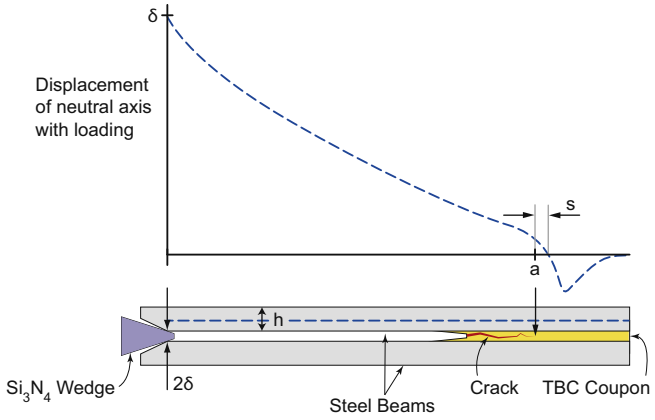

Fig. 2. The DCB configuration (at bottom) and a schematic displacement trace of the mid-line of the steel beam. The offset, *s*, indicates the location of the crack tip relative to the onset of negative displacement (an effect of the compliant foundation, exaggerated here, see also Fig. 4).

region of negative displacements and the crack tip location is, perhaps surprisingly, insensitive to reasonable variations in specimen dimensions and TBC properties. Thus, a simple method is developed to determine the crack length from DIC displacement measurements using a fitting procedure from FE results.

The toughness measurements elucidated by this approach reveal R-curve behavior with steady-state values that are appreciably higher than the initiation toughness. This result and features observed on the fracture surface strongly suggest that a crack bridging and pull-out mechanism, which develops as a consequence of the DVC microstructure, is responsible for the substantial improvement of the TBC's macroscopic resistance to fracture.

2. Experimental approach

Each DCB specimen was fabricated by sandwiching a TBC between two steel beams. Freestanding APS-DVC coatings (kindly provided by GE Energy), 25.4 mm × 25.4 mm × 1 mm, were impregnated with M-bond 610 epoxy (Vishay Micro-measurements) to minimize damage during sample preparation. A surface grinder with a 400 grit diamond wheel established flat, parallel surfaces. The coatings were subsequently sectioned into beams (25.4 mm × 6.35 mm × 1 mm) using a diamond blade and the epoxy was removed by oxidative decomposition in air at 700 °C.

To ensure adequate adhesion, the surfaces of two 304 stainless steel cantilevers (63.5 mm × 6.35 mm × 3 mm) were first ground and then cleaned with acetone. A rubber-toughened adhesive film (FM-1000 from CYTEC Industries) was used to bond the YSZ to one end of the beams. This high viscosity epoxy exhibited minimal

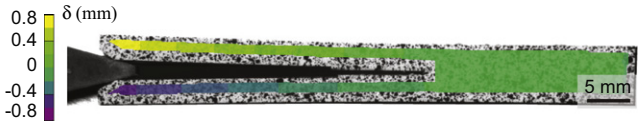

Fig. 3. In situ optical image of a speckled DCB specimen with overlaid displacement contours from digital image correlation measurements.

infiltration into the porous TBC. After curing at 170 °C, subject to a pressure of 180 kPa, the epoxy was limited to an approximately 60 μm thick film at the steel/TBC bond line. A small notch, introduced to the TBC using a diamond wafering blade, assisted crack initiation. During the test, the far end of the specimen was supported on a rigid base, with an intervening, soft metallic foil. At the loading end, a Si_3N_4 wedge, with a 15° half angle, was lubricated with graphite (Crown 8078). Samples were tested at room temperature on a servo-hydraulic test frame (MTS 810) under displacement control.

Images of the specimen were captured at 15–20 s intervals so that the displacement of the cantilevers, including at the location of the wedge (δ), could be measured using DIC (Fig. 3). To facilitate displacement mapping, the assembled specimen was speckled with black on white spray paint. After the experiment was completed, the VIC2D DIC software from Correlated Solutions Inc. compared all images to an initial calibration image taken immediately before testing commenced [27]. The area of interest was defined as the entire speckled surface; the subset size was set to 51 pixels (to reduce noise), the step size was 5 pixels, and the magnification was typically 0.028 ± 0.002 mm/pixel. A series of correlations on unstrained samples established the displacement resolution at better than 1 μm.

3. Calculations

Imaging limitations did not allow for a precise optical determination of the crack tip location and compliance methods were inaccurate for the chosen geometry, resulting in an overestimation of energy release rate. Numerical analysis, through FE simulations in ABAQUS/CAE, facilitated accounting for complex interactions such as the extent of deviations from Bernoulli–Euler beam theory (for one, shear effects at the crack tip) and the presence of the compliant foundation [28–30]. As such, a 2D FE model was utilized to provide values of energy release rate for a set of geometric (lengths: L_{steel}, L_{TBC} and thicknesses: h_{steel}, h_{TBC}) and elastic (E_{steel}, E_{TBC}[1]) parameters, a given crack length (a), and opening displacement at the load point (δ).

[1] E_{TBC} is actually an effective modulus that combines the contributions of the TBC and the epoxy.

The information extracted from the experiment was the displacement as a function of position along the mid-line of the steel beam, collected as δ increased. There remained a challenge in translating the experimental data, which provided values of δ but not a, into FE inputs. Given a rigid foundation, such as in conventional beam theory, the crack tip's position is that of the zero deflection of the beam. However, using this displacement metric to determine crack length results in erroneously high values when a compliant foundation is present. For a beam on an elastic foundation, the zero crossing and succeeding region of negative displacement (Fig. 2) are useful if a relationship between the location of these features and the crack tip is known. A FE study was performed to determine the sensitivity of the zero crossing on specimen dimensions and properties.

A symmetric FE model was created with physical dimensions matching those of half the experimental specimen (one steel beam and 1/2 thickness of the TBC), and meshes were tested for convergence. An independent epoxy layer was not included; instead, adjacent nodes in the steel and TBC were tied. The contribution of the epoxy's low modulus was accounted for by combining it with the TBC's elastic properties into an effective uniaxial modulus, E_{TBC}. Boundary conditions prevented rigid body translations of the steel beam. Meshes of the steel and TBC contained 288×15 and 1320×26 plane stress elements, respectively. The elastic modulus of the steel beam was defined to be 193 GPa and an estimated modulus was assigned to the TBC. Since the properties of the heterogeneous DVC coating are not fully understood, the modulus was used as a parameter in the sensitivity study. Ten cases were analyzed, with E_{TBC} ranging from 10−200 GPa, where the upper bound corresponds to the modulus of dense 8YSZ and the lower bound to the modulus of a laminated composite of 10% epoxy and 90% dense zirconia [31–33]. A representative load point displacement of $\delta = 0.5$ mm was used for the entire sensitivity study; the elastic analysis makes the specific value chosen immaterial, as displacements will scale linearly with the load point displacement. The crack grew from the start of the TBC in increments of $0.1 \cdot L_{TBC}$, and at each crack length, displacements along the midline of the steel beam were recorded.

As expected, plots of displacement as a function of position exhibited a region of negative displacement due to the elastic foundation, as illustrated schematically in Fig. 2. Since crack length was prescribed in these FE simulations, its value could be related to the characteristic features of the region of negative displacement, such as its onset, length, or minimum value. It was determined that it is most reliable to use the position where the beam displacement is zero, preceding the displacements becoming negative. The distance between the location of the crack tip and the onset of the region of negative displacements is henceforth referred to as s (Fig. 2). The sensitivity study examined how s is influenced by parameters in the FE model. Knowledge of variation in s was necessary in order to apply this offset to experimental data and be confident in the extracted values of crack length.

For a given set of dimensions and material properties, there was a characteristic value of s which was constant until the crack reached the last $\approx 30\%$ of the length of the TBC.[2] Uncertainty in s arose from variability in parameters that are not well known or easily measured, specifically the TBC modulus. As E_{TBC} was varied from 10−200 GPa, s was consistently within the range of 1.14−2.31 mm for the chosen geometry. Remembering that crack length was measured from the load point, this range in s translated to a maximum of a 3.3% difference between possible crack lengths. While the behavior near the crack tip was heavily influenced by the compliant foundation, the minimal sensitivity of s (and by extension, crack length) to modulus within the applicable range, was due to the bending stiffness of the steel beams dominating the deformation of the rest of the specimen. As such, knowledge of the exact TBC modulus was not critical. Since utilization of the sensitivity study's results requires experimental data, this procedure is described in Section 4. As will be illustrated, using $E_{TBC} = 25$ GPa as an effective modulus of the TBC/epoxy bilayer resulted in a good match between the simulations and experiments; the characteristic offset value for these conditions is $s = 1.77$ mm.

4. Results

Displacement data was extracted from the centerline of the beams in all images using the crack opening displacement (COD) tool in the VIC2D program. From each of these data sets, a Mathematica script discerned the displacement at the load point, δ, and the position of the first zero crossing. The s offset value was subtracted from this position to determine the location of the crack tip, a. Thus, there were (δ, a) pairs associated with each image, and these pairs were used as inputs for the FE simulations. To verify that the FE model was accurately representing the experiment, each resulting displacement trace from the simulation was then compared to that from the image it represented (Fig. 4). The close match to what was seen experimentally for the same value of δ suggests that the s offset calculation had correctly predicted the crack length.

The macroscopic energy release rate (i.e. driving force) was calculated from the FE results using the well established J-integral [34] (available as a tool in ABAQUS), under the assumption that the fracture process zone is small relative to the crack length. Plotting these TBC toughness values against the calculated crack lengths produced an R-curve.

Nine specimens were fabricated from three standard DVC coatings (three each), and out of these samples, there were six successful experiments where the crack propagated primarily within the TBC. In three cases, the experiment was ideal (these cracks did not deviate into the TBC/epoxy interface); this behavior occurred in one specimen from each of the three coupons (Fig. 5a). Crack growth resistance increased for extensions of about 5 mm and then attained a steady-state of $G_{ss} \approx 300-400\ \mathrm{J/m^2}$. The other successful experiments exhibited a few discrete zones of delamination between the coating and epoxy (Fig. 5b), but the majority of the failure did occur within the TBC. Error, represented in Fig. 5c, includes uncertainties from the measurements of position along the steel beam and calibration value, noise in the DIC data, and slight deviations from the ideal specimen geometry that was used in the sensitivity study determination of the offset, s. To demonstrate the insensitivity of the measured toughness to E_{TBC} and s, multiple simulations were run for one experimental data set. There was not a significant difference in steady-state values, regardless of the exact value of E_{TBC}, within the applicable range of 10−200 GPa, or whether s was appropriately adjusted to match the TBC modulus (Fig. 6).

The steady-state energy release rates from the specimens with some adhesive failure fell within the range defined by the more ideal tests. Furthermore, the toughness behavior of the specimens from each coupon followed similar trajectories. The range in steady-state values was due to typical variations in microstructure

[2] Knowledge of the value of s at longer crack lengths has been characterized, but was not relevant since the experimental data sampling rate was too low to capture the rapid propagation of the crack once it approached the end of the beam.

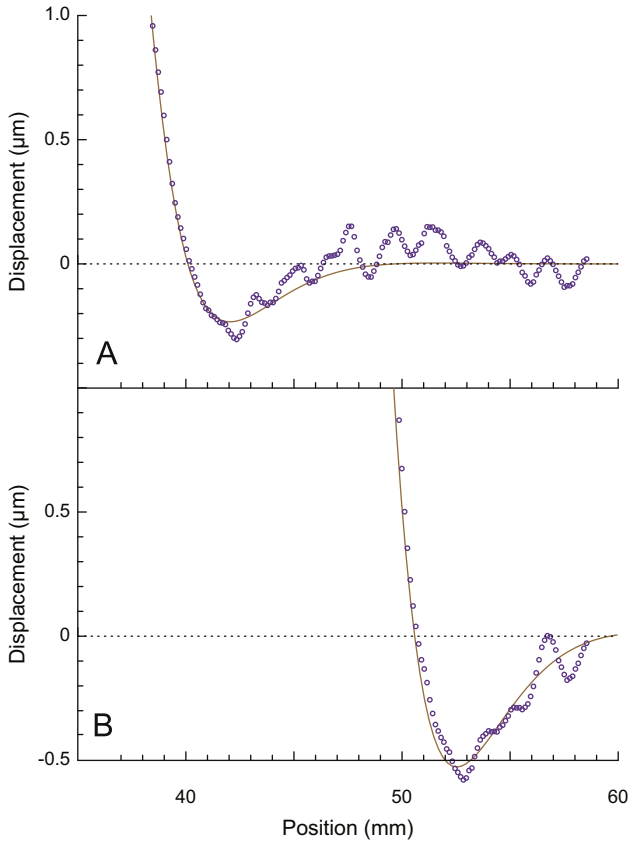

Fig. 4. (a) Displacement of the steel beam's neutral axis in the early stage of crack growth and (b) as the crack nears the end of the beam. In both cases, the traces of simulation results are overlaid on the experimental data points. The compressive region ahead of the crack tip is a manifestation of the significant compliance in the foundation of the beam, i.e. the TBC layer.

across different coatings, rather than small variations that arise from uncontrolled factors in the test.

Complementary fracture surfaces (Fig. 7a) revealed extensive pull-out of the DVC columns. Visual inspection showed that pillars were on the fracture surface associated with the top of the coating (Fig. 7b), while sockets were present on the substrate side. Reminiscent of fiber pull-out in composites [35], it was surmised that the associated frictional dissipation contributed significantly to the toughness. Features on these surfaces were characterized by optical profilometry (Veeco Wyko NT100).

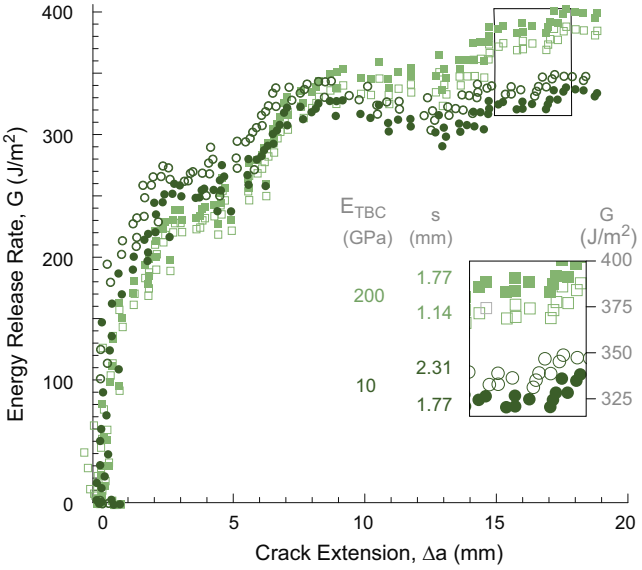

Fig. 6. Toughness values are insensitive to plausible variations of E_{TBC} and s. Multiple simulations on one experimental data set (TBC coupon #2 in Fig. 5) result in steady-state toughness values within experimental scatter.

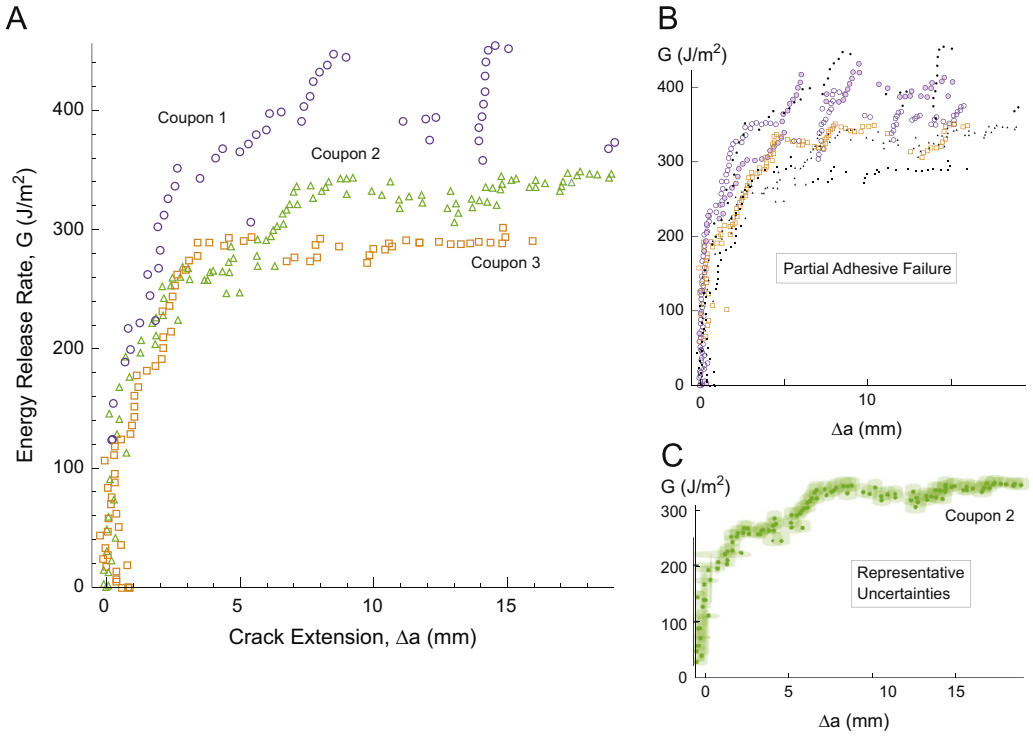

Fig. 5. (a) Measurement of the energy release rate as the crack advances exhibits R-curve behavior, with steady-state toughness values of $G_{ss} \approx 300-400\ \mathrm{J/m^2}$. (b) In cases of partial adhesive failure, repeatable results are attained with toughness values falling entirely within the range established by the more ideal experiments. (c) Calculation uncertainties, representative values shown here for a single sample, are less than the experimental scatter.

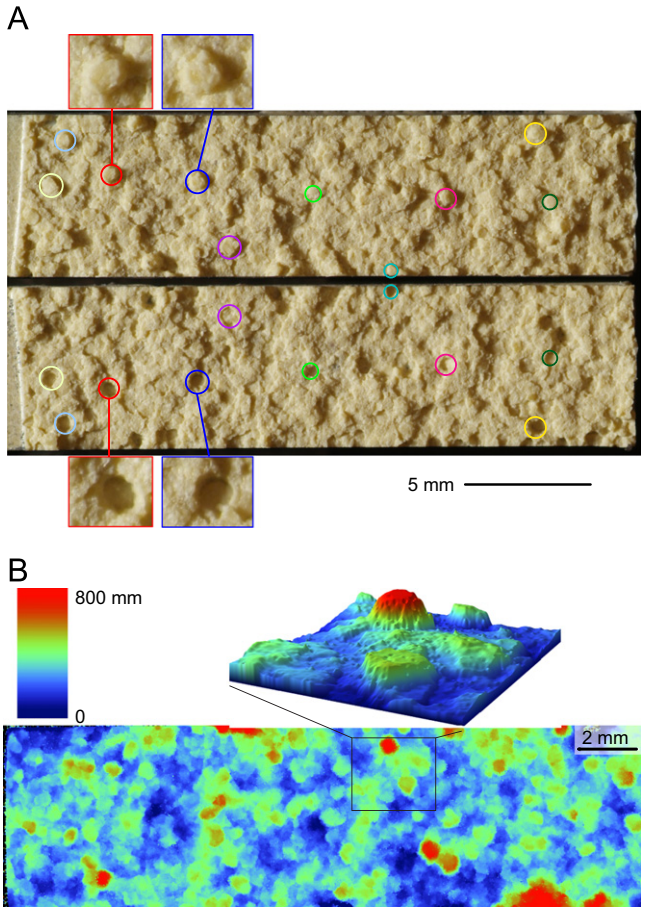

Fig. 7. Visual evidence of a bridging mechanism. (a) Optical micrograph of complementary fracture surfaces of a DVC coating after a DCB test with highlighted pillars and corresponding sockets. (b) Surface topography produced by profilometry, including a detail of a small region containing a pillar with a diameter approximately equivalent to the DVC spacing and an approximate height of half the coating thickness.

In order to probe the operability of the ferroelastic mechanism considered responsible for the superior toughness of tetragonal 7-8YSZ, a comparison was made between X-ray diffraction (XRD) measurements (Panalytical XPERT MPD Powder Diffractometer) performed on a fracture surface and on the top surface of an unmodified TBC. A substantial change in relative intensities between orthogonal reflections in the {002}, {113}, and {004} systems, indicative of an enhanced population of [001] tetragonal domains oriented normal to the surface, was evident after fracture (Fig. 8) [36].

5. Discussion

The salient finding of this investigation, beyond the demonstration that the toughness of porous, microcracked coatings can be rigorously quantified using a DCB/DIC approach, is the observation of toughness values much higher than those measured by conventional microindentation methods on dense samples of the same composition, which are of order $G_0 \approx 40 \pm 5$ J/m^2 [20].[3] This elevated steady-state toughness can be rationalized by a crack bridging and pull-out micromechanical phenomenon wherein the DVC columns act in a manner similar to aligned fibers in a composite [35,39]. In essence, the mechanism is envisaged to proceed as follows (Fig. 9): the crack propagates sampling the strength of the putative pillars (Fig. 9a), fracturing the weaker ones and deflecting at the open boundaries adjacent to the stronger pillars (Fig. 9b), which form bridges across the crack. As the crack continues to open, the stress in any given bridging pillar eventually meets the fracture condition for a critical flaw, often causing failure remote from the crack plane [35]. Those pillars then pull out of their sockets with substantial frictional dissipation at their boundaries [35,40]. Relative displacements of the pillars and the tractions they exert on the crack faces are governed by the friction stress, τ, at the column interfaces (Fig. 9c).

The analysis by Suo et al. [41] on the R-curves resulting from bridging mechanisms is used to calculate the effective bridging stress (σ_0) and the critical opening for loss of bridging traction (δ_0). These two quantities, coupled with the pillar geometry, can be used to estimate the friction stress through a standard shear lag analysis of pillar pullout. (This analysis must yield plausible values of τ to substantiate the above mechanism.) Since the R-curve produced from the current work resembles the case Suo presents for application of a pure moment, which achieves steady-state, the equations for rigid plastic bridging corresponding to that configuration were employed. The superposition of stresses and displacements arising from the applied moment and the bridging mechanism produces the following expressions:

$$\sqrt{G_{ss}} = \sqrt{G_0} + \frac{a_1}{2}\sqrt{C}L_{ss}^2\sigma_0 \tag{1}$$

$$\delta_0 = a_1 L_{ss}^2 \sqrt{CG_{ss}} - \frac{a_1^2}{4} L_{ss}^4 C\sigma_0 \tag{2}$$

where G_{ss} is the steady-state toughness, G_0 is the intrinsic toughness, a_1 is a computed coefficient dependent on specimen geometry and stiffness, C is the beam compliance, and L_{ss} is the steady-state bridging zone size. Values for G_{ss}, G_0, and L_{ss} are extracted from G vs a curves (Fig. 5), such that the bridging parameters δ_0 and σ_0 can be inferred from these equations for a given traction-displacement bridging law.

Regardless of whether the rigid plastic or softening bridging is assumed for the five samples analyzed by surface profilometry, δ_0 is calculated to be 40 ± 20 μm. The features of one fracture surface were measured individually, and the average pillar height is 3–4 times greater than the calculated δ_0 values. It is hypothesized that the initially torturous interfaces of the intact DVC pillars lead to some comminution of the material during pullout, contributing to the sliding stress and amount of frictional dissipation. After sliding about 40 μm, the interfaces become smooth resulting in decreased contact with each other and effective loss of bridging traction.

While δ_0 exhibits no dependence on whether the bridging is rigid plastic or softening, σ_0 is affected, with a mean value of 5.7 MPa in the former case and 11.3 MPa in the latter. To evaluate whether or not such a bridging stress is plausible, it is instructive to calculate the effective sliding stress between pillars that would have to be present to generate stresses of this magnitude. Assuming a constant frictional sliding stress during pull-out and small displacements, equilibrium implies [35,40,42]

$$\sigma_0 = \frac{2h\tau}{R} f \tag{3}$$

[3] The comparison is made here only to highlight the order of magnitude of the difference since the microindentation value is often cited as the intrinsic toughness of the dense material. The latter, however, may vary depending on composition and microstructure [21,20,37,38] but there is no precedent for the values reported here. The relevance of the intrinsic toughness to the fracture process is addressed later in the discussion.

(*footnote continued*)

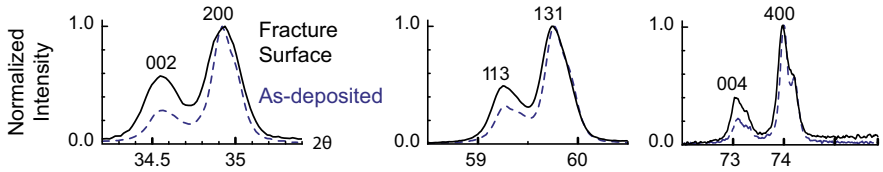

Fig. 8. XRD showing the redistribution in the relative population of tetragonal domain orientation on the fracture surface is suggestive of ferroelastic switching. The population of domains with their *c*-axis oriented along the crack normal increases during the fracture process.

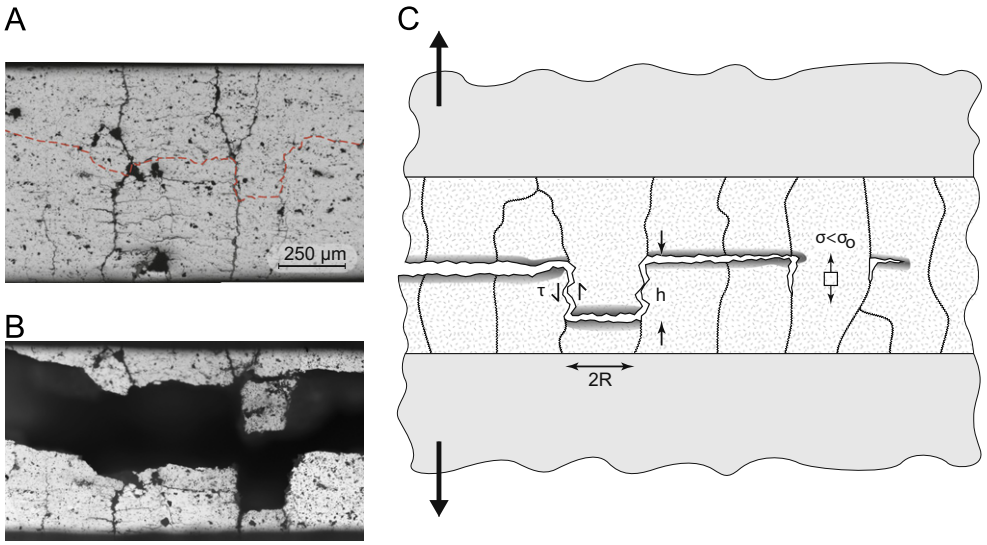

Fig. 9. Cross-sectional views of the same portion of a TBC (a) before (with the eventual crack path indicated by the dashed line) and (b) after fracture reveal the relationship between the vertical cracks in the starting microstructure and the size of a pillar. (c) Illustration of the development of crack bridges and pull-out in a DVC microstructure. The propagating crack follows the path of least resistance, occasionally deflecting at the DVCs and creating pillars in the wake. Upon failure, the pillars undergo frictional pull-out, contributing to an increase in toughness.

where R and h are the nominal radius and height, respectively, of the pillars, f is the area fraction of the fracture surface that experiences pull-out and τ is the frictional sliding stress. This expression for σ_0 can be further simplified by noting that the area fraction of pillars can be expressed as

$$f = \frac{n\pi R^2}{A} \tag{4}$$

where A is the area of the crack plane and n is the number of pillars on the surface. The bridging stress is then given by

$$\sigma_0 = \frac{n2\pi Rh\tau}{A} \tag{5}$$

Optical profilometry data (Fig. 7b) provides values for the total area of the fracture surface (including both the sides and plateaus of the pillars) and the projected area, A; the difference between these measured values is equal to the area of the pillar *sides*, which is the relevant surface for frictional pull-out ($n2\pi Rh$). Using the calculated σ_0 values, it is determined that $\tau \approx 5-38$ MPa, with a mean of 13 MPa. While direct measurements of pull-out stress are required to determine the sliding stress, this inferred friction stress is quite plausible, considering values calculated for other systems [43,44]. The consistency between the deduced pull-out distance and height of the pillars, as well as a reasonable level of sliding stress, lends strong support to the hypothesis of a frictional bridging mechanism.

Concomitant to the bridging mechanism, ferroelastic switching may provide additional toughening that also manifests as R-curve behavior, due to the evolution of a process zone surrounding the crack tip. One may estimate that the steady-state increase in toughness associated purely with switching is of the order of that observed between dense compacts of cubic and tetragonal (t') zirconia, ≈ 40 J/m^2 [20,21], which is much less than the enhancement observed in the experiments. The interplay between the bridging mechanism associated with the columnar microstructure and the ferroelastic contribution arising from the switching of tetragonal domains in the process zone is not fully understood at this time. One may hypothesize, however, that a higher intrinsic toughness would increase the stress necessary to advance the crack tip even in the absence of bridging effects and/or, more importantly, increase the average pull-out length and the bridging effect. In essence, for a given flaw distribution a higher intrinsic toughness would, in principle, require sampling a larger volume of material in each pillar before activating a crack, or if the pillar is already broken at a distance away from the main crack plane, it can withstand the pull-out process without fracturing again under the applied stress. The key point is that determination of bridging effectiveness requires considerations of the microstructural segmentation, the intrinsic toughness, and the flaw distribution. Research is in progress to help elucidate these issues and will be reported in future publications.

6. Conclusion

A refined DCB experimental procedure and analysis is developed and this high-fidelity method can be exploited to accurately measure the toughness of freestanding thin films. The measured mode I toughness of APS coatings with the DVC microstructure has an unexpectedly high steady-state value of 300−400 J/m^2. Auspiciously,

this elevated energy release rate is consistent with toughening mechanisms based on bridging and frictional dissipation, enabled by a combination of the microstructural architecture and an increased intrinsic toughness through ferroelastic switching, which correspond to features observed on the fracture surfaces. Thus, it is inferred that the segmented microstructure has a significant and positive impact on the long-crack toughness of TBCs.

Acknowledgments

This investigation was financially supported under Grants DMR-0605700 and DMR-1105672 from the National Science Foundation. Additional support for EMD through the GAANN fellowship program from the Department of Education is gratefully acknowledged. The research made use of the UCSB MRL Central Facilities, which are supported by the MRSEC Program of the NSF under Award No. DMR-1121053; a member of the NSF-funded Materials Research Facilities Network (http://www.mrfn.org). The authors are grateful to Drs. D.M. Lipkin (GE-GRC) and C.A. Johnson (GE-GRC) for insightful discussions, to Dr. W.A. Nelson (GE-Energy) for providing the coatings examined in this study, and especially to the late professor A.G. Evans who was instrumental in motivating this work.

References

[1] R.A. Miller, J. Therm. Spray Technol. 6 (1997) 35–42.
[2] A.G. Evans, D.R. Clarke, C.G. Levi, J. Eur. Ceram. Soc. 28 (2008) 1405–1419.
[3] R.A. Miller, C.E. Lowell, Thin Solid Films 95 (1982) 265–273.
[4] A.G. Evans, D.R. Mumm, J.W. Hutchinson, G.H. Meier, F.S. Pettit, Prog. Mater. Sci. 46 (2001) 505–553.
[5] V.K. Tolpygo, D.R. Clarke, Acta Mater. 52 (2004) 5115–5127.
[6] V.K. Tolpygo, D.R. Clarke, Acta Mater. 52 (2004) 5129–5141.
[7] D.S. Balint, J.W. Hutchinson, J. Mech. Phys. Solids 53 (2005) 949–973.
[8] X. Chen, R. Wang, N. Yao, A.G. Evans, J.W. Hutchinson, R.W. Bruce, Mater. Sci. Eng. A: Struct. Mater. Prop. Microstruct. Process. 352 (2003) 221–231.
[9] X. Chen, M.Y. He, I. Spitsberg, N.A. Fleck, J.W. Hutchinson, A.G. Evans, Wear 256 (2004) 735–746.
[10] A.G. Evans, N.A. Fleck, S. Faulhaber, N. Vermaak, M. Maloney, R. Darolia, Wear 260 (2006) 886–894.
[11] R.G. Wellman, J.R. Nicholls, J. Phys. D: Appl. Phys. 40 (2007) R293–R305.
[12] M.P. Borom, C.A. Johnson, L.A. Peluso, Surf. Coat. Technol. 86 (1996) 116–126.
[13] S. Kramer, S. Faulhaber, M. Chambers, D.R. Clarke, C.G. Levi, J.W. Hutchinson, A.G. Evans, Mater. Sci. Eng. A: Struct. Mater. Prop. Microstruct. Process. 490 (2008) 26–35.
[14] A.G. Evans, J.W. Hutchinson, Surf. Coat. Technol. 201 (2007) 7905–7916.
[15] J.M. Drexler, A. Aygun, D.S. Li, R. Vassen, T. Steinke, N.P. Padture, Surf. Coat. Technol. 204 (2010) 2683–2688.
[16] G.N. Heintze, R. McPherson, Surf. Coat. Technol. 34 (1988) 15–23.
[17] G.N. Heintze, R. McPherson, Surf. Coat. Technol. 36 (1988) 125–132.
[18] Z.X. Chen, L.H. Qian, S.J. Zhu, Eng. Fract. Mech. 77 (2010) 2136–2144.
[19] A.H. Bartlett, R. Dalmaschio, J. Am. Ceram. Soc. 78 (1995) 1018–1024.
[20] T.A. Schaedler, R.M. Leckie, S. Kramer, A.G. Evans, C.G. Levi, J. Am. Ceram. Soc. 90 (2007) 3896–3901.
[21] C. Mercer, J.R. Williams, D.R. Clarke, A.G. Evans, Proc. R. Soc. A: Math. Phys. Eng. Sci. 463 (2007) 1393–1408.
[22] T.A. Taylor, D.L. Appleby, A.E. Weatherill, J. Griffiths, Surf. Coat. Technol. 43–44 (1990) 470–480.
[23] J.C. Schaeffer, R.W. Bruce, European Patent EP1281788 (2003).
[24] H.B. Guo, R. Vassen, D. Stover, Surf. Coat. Technol. 192 (2005) 48–56.
[25] M. Karger, R. Vassen, D. Stoover, Surf. Coat. Technol. 206 (2011) 16–23.
[26] T.A. Taylor, Surf. Coat. Technol. 54 (1992) 53–57.
[27] M.A. Sutton, J.J. Orteu, H.W. Schreier, Image Correlation for Shape, Motion and Deformation Measurements: Basic Concepts, Theory, and Applications, Springer, New York, 2009.
[28] P. Ostojic, R. McPherson, J. Am. Ceram. Soc. 71 (1988) 891–899.
[29] M.F. Kanninen, Int. J. Fract. 9 (1973) 83–92.
[30] M.F. Kanninen, Int. J. Fract. 10 (1974) 415–430.
[31] J. Malzbender, R.W. Steinbrech, J. Mater. Res. 18 (2003) 1975–1984.
[32] T. Wakui, J. Malzbender, R.W. Steinbrech, J. Therm. Spray Technol. 13 (2004) 390–395.
[33] T. Wakui, J. Malzbender, R.W. Steinbrech, Surf. Coat. Technol. 200 (2006) 4995–5002.
[34] B.R. Lawn, Fracture of Brittle Solids, second ed., Cambridge University Press, Cambridge, 1993.
[35] M.D. Thouless, A.G. Evans, Acta Metall. 36 (1988) 517–522.
[36] J.F. Jue, A.V. Virkar, J. Am. Ceram. Soc. 73 (1990) 3650–3657.
[37] F.M. Pitek, C.G. Levi, Surf. Coat. Technol. 201 (2007) 6044–6050.
[38] A. Loganathan, A.S. Gandhi, Mater. Sci. Eng. A: Struct. Mater. Prop. Microstruct. Process. 556 (2012) 927–935.
[39] A.G. Evans, J. Am. Ceram. Soc. 73 (1990) 187–206.
[40] D.B. Marshall, B.N. Cox, A.G. Evans, Acta Metall. 33 (1985) 2013–2021.
[41] Z. Suo, G. Bao, B. Fan, J. Mech. Phys. Solids 40 (1992) 1–16.
[42] B. Budiansky, J.W. Hutchinson, A.G. Evans, J. Mech. Phys. Solids 34 (1986) 167–189.
[43] D.B. Marshall, A.G. Evans, J. Am. Ceram. Soc. 68 (1985) 225–231.
[44] R.N. Singh, J. Am. Ceram. Soc. 72 (1989) 1764–1767.